TITLE: Radiographic protocol and normal anatomy of the hind feet in the white rhinoceros (ceratotherium simum)

AUTHORS: Robert J. Dudley, Simon P. Wood, John R. Hutchinson, Renate Weller

JOURNAL TITLE: VETERINARY RADIOLOGY & ULTRASOUND

PUBLISHER: Wiley

PUBLICATION DATE: March/April 2015

DOI: 10.1111/vru.12215

Development of a Radiographic Protocol for White Rhinoceros (*Ceratotherium simum*) Hind Feet and a Description of Their Normal Radiographic Anatomy

Robert J. Dudley, Simon P. Wood, John R. Hutchinson, Renate Weller

Key words: x-ray, Rhinocerocerotidae, pes, medical imaging, morphology

Running head: Radiography of the White Rhinoceros Pes

Funding source: British Biotechnology and Biosciences Research Council, grant number BB/H002782/1

Abstract

Foot pathology is a common and important health concern in captive rhinoceroses worldwide, but osteopathologies are rarely diagnosed, partly because of a lack of radiographic protocols. Here, we aimed to develop the first radiographic protocol for rhinoceros feet and describe the radiographic anatomy of the white rhinoceros (*Ceratotherium simum*) hind foot (pes). Computed tomographic (CT) images were obtained of nine cadaver pedes from seven different white rhinoceroses and assessed for pathology. A single foot deemed free of pathology was radiographed using a range of different projections and exposures to determine the best protocol. The normal radiographic anatomy of the white rhinoceros pes was described using radiographs and 3D models produced from the CT images. An optimal projection was determined for each bone in the rhinoceros pes focusing on highlighting areas where pathology has been previously described. The projections deemed to be most useful were D60Pr-PlDiO (digit III), D45Pr45M-PlDiLO (digit II) and D40Pr35L-PlDiLO (digit IV). The primary beam was centred 5-7cm proximal to the cuticle on the digit of interest. Articular surfaces, ridges, grooves, tubercles, processes and fossae were identified. The radiographic protocol we have developed along with the established normal radiographic anatomy we have described will allow for more accessible and effective diagnosis of white rhinoceros foot osteopathologies.

Introduction

Rhinoceroses (family Rhinocerotidae) are amongst the largest living terrestrial animals, the largest being the white rhinoceros (Ceratotherium simum) at up to 2300 kg body mass.[1] Considering the large size of rhinoceroses it is not surprising that their feet are commonly affected by pathology.[2-5] Soft tissue and hoof diseases of the feet are common and well described.[2, 3, 5, 6] In contrast, documented osteopathies of live rhinoceroses' feet are scarce in the current literature. Arthritis is known to affect older animals[6] or is a potential sequel to trauma.[7] Degenerative arthritis has been documented in a wild black rhinoceros, so these conditions do not solely pertain to captive individuals.[8] Osteomyelitis of the middle phalanx of digit 3 has been reported in an Indian rhinoceros which also had associated arthritis of the distal interphalangeal joint.[9] Osteomyelitis of the second and third phalanges of digit 3 has been reported in one captive Eastern black rhinoceros.[10] The relative lack of diagnosed bone disease compared to soft tissue disease in the current literature is quite striking. We have recently shown by examination of cadaver rhinoceros specimens that bone pathologies are common in rhinoceros feet.[4] Of 27 rhinoceroses studied, 22 showed some degree of osteopathy in at least one limb. Six main osteopathies were found that according to previous literature are rarely if at all diagnosed ante mortem. The main lesions were enthesiophyte formation, osteoarthritis, remodeling, osteitis/osteomyelitis, fracture, and subluxation.[4] Another recent study found significant bone pathology by CT examination of the cadaver feet of two white and one Indian rhinoceros.[11] None of the lesions were diagnosed ante mortem and in some cases the rhinoceroses were euthanased due to diseases of the soft tissue structures of the foot.

There are currently few documented instances of the use of radiography to diagnose rhinoceros foot pathology. Two reports have successfully diagnosed osteomyelitis in rhinoceroses with the aid of radiographs taken under general anesthesia.[9, 10] Another

report took radiographs on multiple occasions of a well-tempered rhinoceros whilst it was sleeping.[12] The discrepancy between post- and ante-mortem diagnosis of bone pathology reflects the apparent infrequency in which diagnostic imaging is used in rhinoceroses due to the difficulty and hazards of performing procedures on conscious rhinoceroses and the risks associated with anesthesia.[7, 8, 13-16] Furthermore the normal radiographic anatomy of rhino feet has not been established and there are currently no radiographic protocols described for rhinoceros feet. Elephant feet are more commonly radiographed and protocols exist for both free contact and protected contact settings.[17,18-20] This is possible because free contact between keepers and elephants has been historically popular, and because captive elephants are often trained to a high level,[21] including being trained to lift their feet for examination and treatment.[22-23] Such training remains rare for captive rhinoceroses.

The most recent figures estimate 750 white rhinoceroses in captivity worldwide and the species is listed as near threatened.[24] Three other rhinoceros species are currently listed as critically endangered and one as vulnerable. [25-28] Captive rhinoceroses serve as an important conservation safety net and are a key source in re-establishing wild populations,[29] monitoring foot health appears essential in maintaining welfare and ensuring their continued existence. The aims of this study were to describe the normal radiographic anatomy of the white rhinoceros hind foot (pes) and to develop a protocol for radiographing standing white rhinoceros' pedes in captivity.

Methods

Nine cadaver white rhinoceros pedes from seven different skeletally mature white rhinoceros individuals were obtained from accredited European zoos and safari parks during the period 2005-2013 and frozen. The clinical history that accompanied each rhinoceros was limited,

and considering the rarity of the specimens we did not have inclusion/exclusion criteria. The feet were thawed and subsequently refrozen for all procedures.

Computed tomography (CT) scans of the pedes were obtained (LightSpeed Ultra 8 Slice, GE Healthcare, Wisconsin, USA). For the scans the pedes were loaded via a custom-made hydraulic jig with 500kg to approximate standing conditions (assuming 20% body weight supported per pes, 30% per manus) of a 2500kg adult white rhinoceros. Continuous images were obtained in a transverse plane perpendicular to the long axis of the limb. Image slices were obtained at a slice thickness and distance of 1.3mm and exposures varied according to specimen size.

The DICOM format CT images of all cadaver feet were imported into a three-dimensional (3D) rendering program (Mimics® version 10.11, Materialise, Belgium). Individual bones were isolated using grey-scale thresholding with manual correction and were subsequently rendered into 3D models. The raw CT images and the 3D models were subjectively evaluated for the presence of pathology and a specimen that was deemed representative of normal morphology was selected. The 3D models of each phalanx from this specimen were exported as high resolution STL files into another 3D rendering program (Meshlab® version 1.3.2, Italian National Research Council, Rome), where they were then converted to Collada format for compatibility with graphics editing software (Adobe Photoshop CC version 14.2, Adobe Systems, California).

The same cadaver specimen was used for development of the radiographic protocol and collection of radiographs to describe normal radiographic anatomy. The majority of rhinoceroses are not trained to lift their feet[13, 30-32] and our discussions with rhinoceros keepers highlighted that most rhinoceros will not tolerate cassettes around their legs for dorsoplantar or lateromedial views, so for clinical relevance the radiographic projections trialed were limited to dorsoproximal-plantarodistal obliques, dorsoproximolateral-

plantarodistomedial obliques and dorsoproximomedial-plantarodistolateral obliques, all of which require the rhinoceros standing on a cassette tunnel. To approximately replicate standing conditions the pes was placed on a cassette tunnel and again loaded with 500 kg via a hydraulic jig. Radiographs were acquired using a high powered ceiling mounted X-ray generator (Polydoros, Siemens Medical, Erlangen, Germany) and a digital processing system (FCR XG5000, Fujifilm, Tokyo, Japan) with a source to image distance of 80 cm. Digit III was radiographed with dorsoproximal-plantarodistal projections ranging from 30° to 80° at 5° intervals. The same procedure was followed with digits II and IV although with an added element of differing medial and lateral obliquity, respectively. Various exposure settings were tried for each bone. The radiographs were then assessed for diagnostic quality by a large animal veterinary radiology specialist (RW). Assessment criteria focused on visualization of gross anatomic features and visibility of areas where pathology has been previously identified.[4, 11]

As a pictorial representation of radiographic anatomy the 3D reconstructions in Collada format were superimposed on top of the selected radiographs using the graphics editing program and labeled. Where radiograph images were distorted due to obliquity of the primary beam relative to the cassette it was necessary to either scale or to use a warping tool on the radiograph image to facilitate the accurate superimposition of the 3D model.

Results

Radiographic protocol

Table 1 shows the ideal projections for each bone of the rhinoceros pes. The pes is positioned on the cassette tunnel with the cassette positioned orthogonal to the axis of the primary beam but parallel to the ground. To account for the obliquity of the beam the digit of interest is positioned on the near edge of the cassette tunnel (Figs. 1 and 2). For centering on the distal

interphalangeal joint the primary beam is centered on the proximal border of the cuticle. For centering on the proximal interphalangeal joint the beam is centered 7 cm proximal to the cuticle (5 cm for digit II and IV), this was found to be best for including the whole digit. Exposures of 90 kV and 20 mAs were found to result in diagnostic images achievable with a portable x-ray machine.

It was found that the optimal projections for the middle phalanx of each digit also produced images of adequate diagnostic quality of the proximal and distal phalanges, with good visualisation of the interphalangeal joint spaces and minimal bone superimposition. In a clinical setting where time is a factor these three views (D60Pr-PlDiO, D45Pr45M-PlDiLO and D40Pr35L-PlDiLO) would therefore be most appropriate. It is important to note that digits II and IV were not mirror images of one another; there were small conformational differences which resulted in slightly different required projections and images produced.

Radiographic anatomy

Figure 3 shows a complete 3D model of the pes that was radiographed. Evaluation of all the specimen's CT images showed each pes to contain 3 metatarsal bones and corresponding digits (although one pes had an amputation of digit IV at the proximal interphalangeal joint). Each digit contained a proximal, middle and hoof-shaped distal phalanx. The middle digit (III) was largest in all specimens. In each digit the proximal phalanx was the longest and distal phalanx the shortest. The distal phalanges were the widest and terminated in weight-bearing solar surfaces. The distal phalanx of digit III had bilateral plantar processes projecting abaxially whilst the distal phalanges of digits II and IV had only a single plantar process projecting abaxially. Paired proximal sesamoid bones were present on the distal plantar surface of each metatarsal bone. No distal sesamoid bones were present in any of the specimens. As previously shown, nutrient foramina were present in all bones[5] and slightly

varied by location and number between specimens. They were most abundant in the distal phalanges especially of digit III. All specimens had a large foramen within the plantar process of the distal phalanges of digits II and IV. All anatomic details labelled in Figures 4-11 were found to be generally consistent in all specimens and thus were deemed normal.

Figures 4-11 show the normal radiographic anatomy of a skeletally mature white rhinoceros pes. The radiographs described above are displayed both alone and superimposed with the 3D models produced from CT images. The 3D models are overlaid twice in order to show details of the dorsal aspect and plantar aspect of each bone. The images are displayed side by side to facilitate appreciation of the anatomy.

The images include the distal metatarsal, proximal phalanx, middle phalanx and distal phalanx of all 3 digits. The proximal sesamoid bones are also visible in some of the images but the radiographs are not of diagnostic quality for these bones. The metatarsophalangeal joints, proximal phalangeal joints and distal phalangeal joints are all radiographically visible, although the conformation of a rhinoceros pes does not allow for complete visualisation of the metatarsophalangeal or distal interphalangeal joint spaces. Visualisation through the proximal interphalangeal joint spaces is possible but can require two views to appreciate the whole joint space.

Discussion

We have described the first radiographic protocol for imaging the entire rhinoceros pes with the rhinoceros standing on a cassette tunnel; there are no prior protocols or detailed radiographic descriptions. The exposures used in the protocol can be produced by a portable X-ray machine with a digital radiography system so it can be reproduced in zoo and field settings. The developed protocol focused on all three phalanges of each digit and their associated joints and focused on sites of pathologies previously identified; thus employment

of this protocol should increase successful diagnosis of osteopathologies in the pedes of rhinoceroses. [4, 11] The protocol and described anatomy are also relevant for use in radiography of anesthetized rhinoceroses. Anatomical knowledge of rhinoceros feet is currently fairly limited. The skeletal anatomy has been previously described[4, 11, 33] and is described in detail by this study; however, knowledge of soft tissue structures in the rhinoceros foot is currently limited. Multiple ridges, grooves, tubercles, and processes have been described in this study, some of which are likely associated with soft tissue attachments. Identification of such attachments would improve appreciation of normal variations of anatomy and assist in diagnosis of specific pathological changes associated with these structures.

Unfortunately we were unable to test the protocol on a live rhinoceros. There is a possibility that the D45Pr45M-PlDiLO projection for digit II may be difficult or not possible in some rhinoceroses. It was our intention to position the X-ray tube on the opposite side of the rhinoceros to the pes of interest and direct the primary beam under the rhinoceros's abdomen to obtain this oblique projection. In those rhinoceroses where the girth of the abdomen or the shortness of the legs is a limiting factor the described projection can serve as a guideline and a shallower angle must be used. Training methods used for rhinoceroses have advanced in recent years. Target training (rhinoceros moves to a target on instruction) is the most commonly employed and is used as a basis for training of other techniques such as chute training, weigh scale training, blood sampling, and foot care. 13,30,31,32 It would be unfeasible with the current training practices to expect the majority of rhinoceroses to lift their feet for positioning as is done for elephant radiography.[20] There is however potential for target-trained rhinoceroses to be trained to walk onto a cassette tunnel for this protocol to be employed, allowing for accessible and simple radiography of conscious rhinoceroses. An option we considered was to produce a large cassette tunnel that fills the whole floor of a

rhinoceros chute. This would simplify training in that the rhinoceros would only have to walk into the chute and stand. A transparent top surface (e.g. polycarbonate) to the cassette tunnel would facilitate visualization and positioning of the cassette relative to the primary beam and the foot. In addition future rhinoceros chutes can be built with gaps for radiography, hence improving image quality and ease of radiograph procurement whilst still maintaining a safe environment for both the animals and the staff. Given the newly recognized prevalence of foot pathologies in rhinoceroses,[4, 11] such improvements to rhinoceros management regimes would be timely and beneficial.

Acknowledgments

Thanks to the rhinoceros keepers at Colchester Zoo for their expert advice on rhinoceros behaviour and training. We thank the editor and two anonymous reviewers for their constructive comments on the earlier draft of this paper. Sophie Regnault gave helpful input during this project, and Thomas Hildebrandt and Robert Hermes provided some specimens.

References

1 Shrader AM, Owen-Smith N, Ogutu JO. How a mega-grazer copes with the dry season: food and nutrient intake rates by white rhinoceros in the wild. Funct Ecol. 2006 April;20(2):376-84.

2 Jacobsen J. A review of rhino foot problems. In: Aubery L, Kennedy J, Gaffney M, Patton L, Slobig C, Mehrdadfar F, editors. Proceedings of the [second] Rhino Keepers' Workshop 2001; 2001 May 7-10; Zoological Society of San Diego. 2002. p. 56-59.

3 Jones DM. The husbandry and veterinary care of captive rhinoceroses. International Zoo Yearbook. 1979;19:239-52.

4 Regnault S, Hermes R, Hildebrandt T, Hutchinson J, Weller R. Osteopathology in the feet of rhinoceroses: lesion type and distribution. J Zoo Wildl med. 2013 Dec;44(4):918-27

5 Von Houwold F. Foot problems in Indian rhinoceroses (Rhinoceros unicornis) in zoological gardens; macroscopic and microscopic anatomy, pathology, and evaluation of the causes. [dissertation]. Zurich: Zurich university; 2001

6 Von Houwald F. Chapter 5: Health. In: Guldenschuh G, Von Houwold F, editors. Husbandry manual for the greater one-horned or Indian rhinoceros (Rhinoceros unicornis). Basel: Basel Zoo; 2002. p. 36-43.

7 Silberman M, Fulton R. Medical problems of captive and wild rhinoceroses: a review of the literature and personal experiences. J Zoo An Med. 1979;10(1):6-16.

8 Wallach JD. Degenerative arthritis in a black rhinoceros. Journal Am Vet Mes Assoc. 1967 Oct 1;151(7):887-9

9 Flach EJ, Walsh TC, Dodds J, White A, Crowe O. Treatment of osteomyelitis in a greater one-horned rhinoceros (Rhinoceros unicornis). Verh ber. Erkrg. Zootiere. 2003;41:1-7

10 Harrison TB, Stanley BJ, Sikarskie JG, Bohart G, Ames NK, Tomlian J, et al. Surgical amputation of a digit and vacuum-assisted-closure (V.A.C.) management in a case of osteomyelitis and wound care in an Eastern black rhinoceros (Diceros bicornis michaeli). J Zoo Wildl Med. 2011;42(2):317-21.

11 Galateanu G, Hildebrandt TB, Maillot A, Etienne P, Potier R, Mulot B, et al. One small step for rhinos, one giant leap for wildlife management- imaging diagnosis of bone pathology in distal limb. PLOS ONE [Internet]. 2013 July 9 [cited 2014 Feb 25]; e668493. doi:10.1371/journal.pone.0068493. Available from: http://www.plosone.org/article/info%3Adoi%2F10.1371%2Fjournal.pone.0068493

12 Mayer CP, Sakefski E. Treatment and management of chronic foot problems in an Indian rhinoceros. Animal Keeper's Forum. 1987 Dec. p. 380-4.

13 Joseph S. Rhino training and enrichment at Disney's Animal Kingdom. In: Mehrdadfar F et al. Proceedings of the First Rhino Keepers' workshop; 1999 May 7-9; Orlando, Florida. p. 111-20.

14 West G, Heard D, Caulkett N. Zoo animal and wildlife immobilization and anesthesia. New Jersey: John Wiley & Sons; 2008 Apr 15. p. 543-66.

15 Bush M, Raath JP, Grobler D, Klein L. Severe hypoxaemia in field-anaesthetised white rhinoceros (Ceratotherium simum) and effects of using tracheal insufflation of oxygen. J S Afr Vet Assoc. 2004;75(2):79-84.

16 Walzer C, Goeritz F, Pucher H, Hermes R, Hildebrandt T, Schwarzenberger F. Chemical restraint and anesthesia in white rhinoceros (Ceratotherium simum) for

reproductive evaluation, semen collection and artificial insemination. In: Proceedings of the American Association of Zoo Veterinarians; 2000. p. 98-101.

17 Miller RE, Fowler ME. Fowler's Zoo and Wild Animal Medicine Current Therapy. Volume 7. Philadelphia: Elsevier Health Sciences; 2011 Jul 11. p. 515-23.

18 Gage LJ. Radiographic techniques for the elephant foot and carpus. In: Fowler ME, Miller RE, editors. Zoo and Wild Animal Medicine: Current Therapy. 4th ed. Philadelphia: W.B. Saunders; 1999. p. 517-20.

19 Kudlas M, Maloy D, George CS. Medical management: Radiographic positioning and techniques for the elephant foot using protected contact. Journal of the Elephant Manager's Association. 2008;19:8-11.

20 Mumby C, Bouts T, Sambrook L, Danika S, Rees E, Parry A, et al. Validation of a new radiographic protocol for Asian elephant feet and description of their radiographic anatomy. Vet Rec [Internet]. 2013 Sep 18 [cited 2014 Feb 25]; doi:10.1136/vr.101696. Available from: http://veterinaryrecord.bmj.com/content/early/2013/09/18/vr.101696.full

21 Desmond T, Laule G. Protected-contact elephant training. Active Environments for AZA Annual Conference [Internet]. 1991 [cited 2014 Feb 25]. Available from: http://activeenvironments.org/pdf/PC_Elephant_Training.pdf

22 West G. Occurence and treatment of nail/foot abscesses, nail cracks, and sole abscesses in captive elephants. In: Csuti BA, Sargent EL, Bechert US, editors. 1st ed. Ames: Iowa State University Press; 2001. p. 93-7.

23 Custi B, Sargent EL, Bechert US. The elephant's foot: prevention and care of foot conditions in captive Asian and African elephants. New Jersey: John Wiler & Sons; 2008 Apr 14.

24 IUCNRedList.org [internet]. Cambridge: International Union for Conservation of Nature Global Species Programme Red List Unit; [cited 2014 Feb 25]. Available from: http://www.iucnredlist.org/details/4185/0. Access 2014 Apr 14.

25 IUCNRedList.org [internet]. Cambridge: International Union for Conservation of Nature Global Species Programme Red List Unit; [cited 2014 Feb 25]. Available from: http://www.iucnredlist.org/details/6557/0.

26 IUCNRedList.org [internet]. Cambridge: International Union for Conservation of Nature Global Species Programme Red List Unit; [cited 2014 Feb 25]. Available from: http://www.iucnredlist.org/details/6553/0.

27 27IUCNRedList.org [internet]. Cambridge: International Union for Conservation of Nature Global Species Programme Red List Unit; [cited 2014 Feb 25]. Available from: http://www.iucnredlist.org/details/19495/0.

28 28IUCNRedList.org [internet]. Cambridge: International Union for Conservation of Nature Global Species Programme Red List Unit; [cited 2014 Feb 25]. Available from: http://www.iucnredlist.org/details/19496/0.

29 Osofsky SA, Paglia DE, Radcliffe RW, Miller RE, Emslie RH, Foose TJ, et al. First, do no harm: a precautionary recommendation regarding the movement of black rhinos from overseas zoos back to Africa. Pachyderm. 2001 Jan-Jun;30:17-23.

30 Cook J. Training Successes with Southern White Rhinoceros at Colchester Zoo. Ratel. 2009 Dec;36(4):5-7.

31 Forsyth S, Row J, Cook J. The benefits of training southern white rhinoceros (Ceratotherium simum simum) at Colchester Zoo. International Zoo News. 2012;59(1):38-42.

32 Pill L, Hange B. Using operant conditioning to weigh 11 Southern white rhinos (Ceratotherium simum simum). Animal Keeper's Forum 2000;27(10):432-435.

33 Flower WH. An introduction to the osteology of the mammalian, 3rd ed. London: Macmillan and Co, 1885; 294–296.

34 Table 1: optimal radiographic projections for visualising each individual bone in the white rhinoceros pes.

Bone	**Projection**
Digit III Proximal Phalanx	D75Pr-PlDiO
Digit III Middle Phalanx	D60Pr-PlDiO
Digit III Distal Phalanx	D40Pr-PlDiO
Digit II Proximal Phalanx	D50Pr45M-PlDiLO
Digit II Middle Phalanx	D45Pr45M-PlDiLO
Digit II Distal Phalanx	D40Pr45M-PlDiLO
Digit IV Proximal Phalanx	D50Pr35L-PlDiLO
Digit IV Middle Phalanx	D40Pr35L-PlDiLO
Digit IV Distal Phalanx	D35Pr35L-PlDiLO

Figure Legends

Figure 1: Positioning and centring for a D60Pr-PlDiO radiograph of the middle phalanx of digit III of a left pes. The pes is being loaded with a hydraulic jig to simulate standing conditions. The primary beam is centred (*) 7cm proximal to the cuticle

84x84mm (300 x 300 DPI)

Figure 2: Positioning and centring for a D45Pr45M-PlDiLO radiograph of the middle phalanx of digit II of a left pes. The pes is being loaded with a hydraulic jig to simulate standing conditions. The primary beam is centred (*) 7cm proximal to the cuticle

84x107mm (300 x 300 DPI)

Figure 3: Dorsal and plantar views of a 3D model of the white rhinoceros left pes. The bones of the tarsus are the: talus, calcaneus, central tarsal bone, 1st tarsal bone, 2nd tarsal bone, 3rd tarsal bone and 4th tarsal bone. Each digit (digits II, III and IV) contains: metatarsal bone, paired proximal sesamoid bones, proximal phalanx, middle phalanx and distal phalanx

173x122mm (300 x 300 DPI)

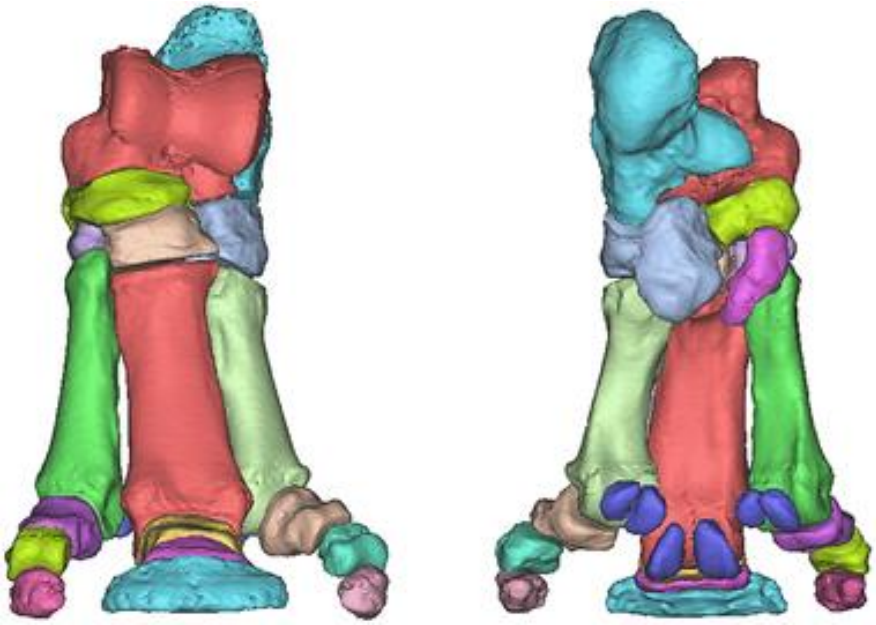

Figure 4: Normal radiographic anatomy of digit III of a white rhinoceros pes, proximal phalanx. DIGIT III: MT Metatarsal, P1 Proximal phalanx, P1d Proximal phalanx dorsal aspect, P1p Proximal phalanx plantar aspect, P2 Middle phalanx, P3 Distal phalanx, S Proximal sesamoid, 1 Metatarsophalangeal joint, 2 Proximal interphalangeal joint, 3 Proximal articular surface, 4 Plantaroproximal edge, 5 Dorsoproximal edge, 6 Medial dorsoproximal tubercle, 7 Lateral dorsoproximal tubercle, 8 Dorsomedial oblique ridge, 9 Dorsolateral oblique ridge, 10 Medial plantaroproximal tubercle, 11 Lateral plantaroproximal tubercle, 12 Transverse plantar ridge, 13 Transverse plantar groove, 14 Distal articular surface, 15 Sagittal groove 173x75mm (200 x 200 DPI)

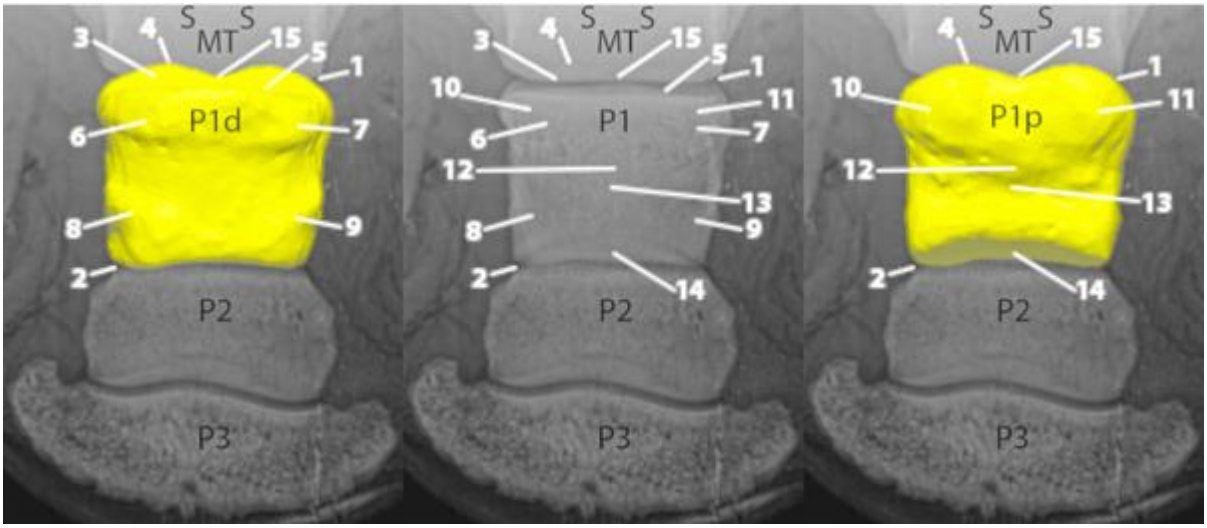

Figure 5: Normal radiographic anatomy of digit III of a white rhinoceros pes, middle phalanx. DIGIT III: S Proximal sesamoid bone, MT Metatarsal, P1 Proximal phalanx, P2 Middle phalanx, P2d Middle phalanx dorsal aspect, P2p Middle phalanx plantar aspect, P3 Distal phalanx, 1 Proximal interphalangeal joint, 2 Distal interphalangeal joint, 3 Proximal articular surface, 4 Plantaroproximal edge, 5 Dorsoproximal edge, 6 Medial condyle, 7 Lateral condyle, 8 Distal articular surface, 9 Medial oblique ridge, 10 Lateral oblique ridge, 11 Dorsal transverse recess, 12 Dorsal transverse ridge, 13 Plantar recess, 14 Medial collateral ligament eminence, 15 Lateral collateral ligament eminence 173x85mm (200 x 200 DPI)

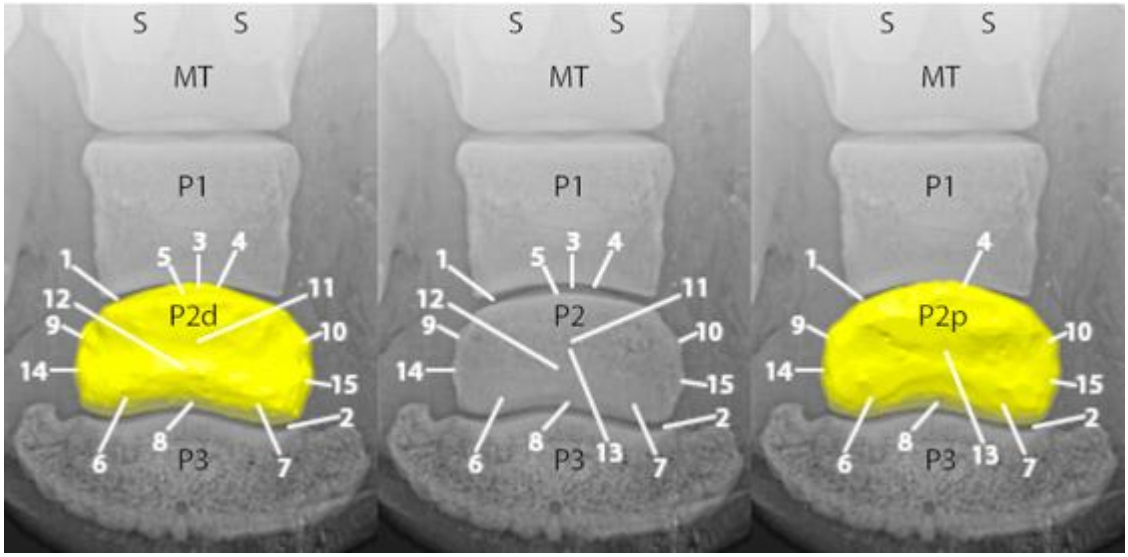

Figure 6: Normal radiographic anatomy of digit III of a white rhinoceros pes, distal phalanx. DIGIT III: P1 Proximal phalanx, P2 Middle phalanx, P3 Distal phalanx, P3d Distal phalanx dorsal aspect, P3p Distal phalanx plantar aspect, 1 Distal interphalangeal joint, 2 Proximal articular surface, 3 Plantaroproximal edge, 4 Dorsoproximal edge, 5 Planum cuneatum (sole surface), 6 Sole border, 7 Extensor process, 8 Flexor surface, 9 Medial parietal sulcus, 10 Lateral parietal sulcus, 11 Medial plantar process, 12 Lateral plantar process, 13 Medial solar foramen, 14 Lateral solar foramen, 15 Nutrient foramina 84x180mm (200 x 200 DPI)

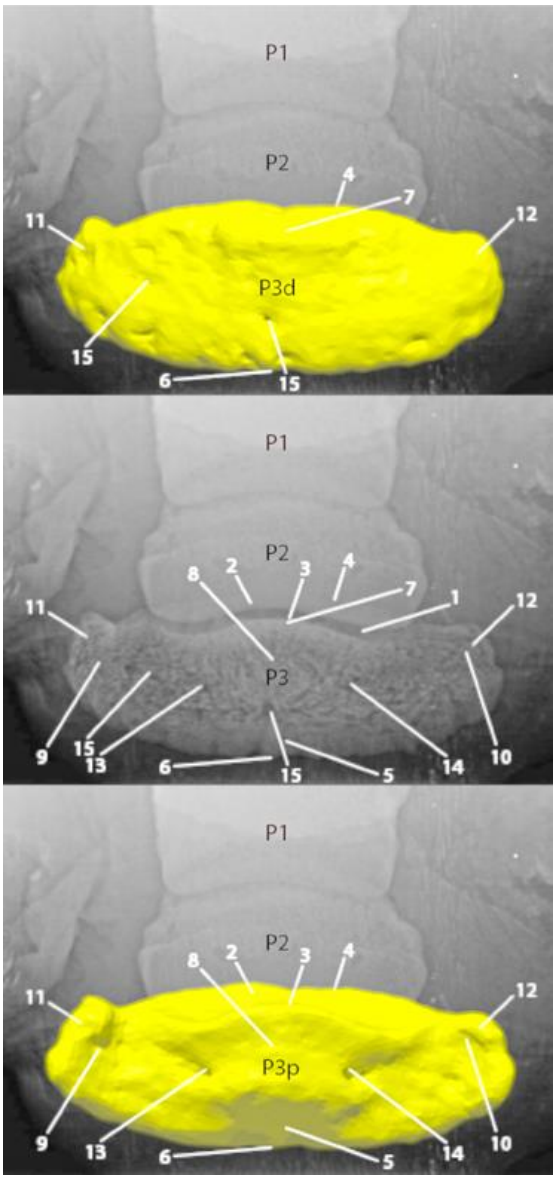

Figure 7: Normal radiographic anatomy of digit II of a white rhinoceros pes, proximal phalanx. DIGIT II: MT Metatarsal, P1 Proximal phalanx, P1d Proximal phalanx dorsomedial aspect, P1p Proximal phalanx plantaromedial aspect, P2 Middle phalanx, P3 Distal phalanx, S Proximal sesamoid, 1 Metatarsophalangeal joint, 2 Proximal interphalangeal joint, 3 Proximal articular surface, 4 Plantaroproximal edge, 5 Dorsoproximal edge, 6 Medial dorsoproximal tubercle, 7 Lateral dorsoproximal tubercle, 8 Dorsomedial oblique ridge, 9 Dorsolateral oblique ridge, 10 Medial plantaroproximal tubercle, 11 Lateral plantaroproximal tubercle, 12 Transverse plantar ridge, 13 Transverse plantar groove, 14 Distal articular surface 173x73mm (200 x 200 DPI)

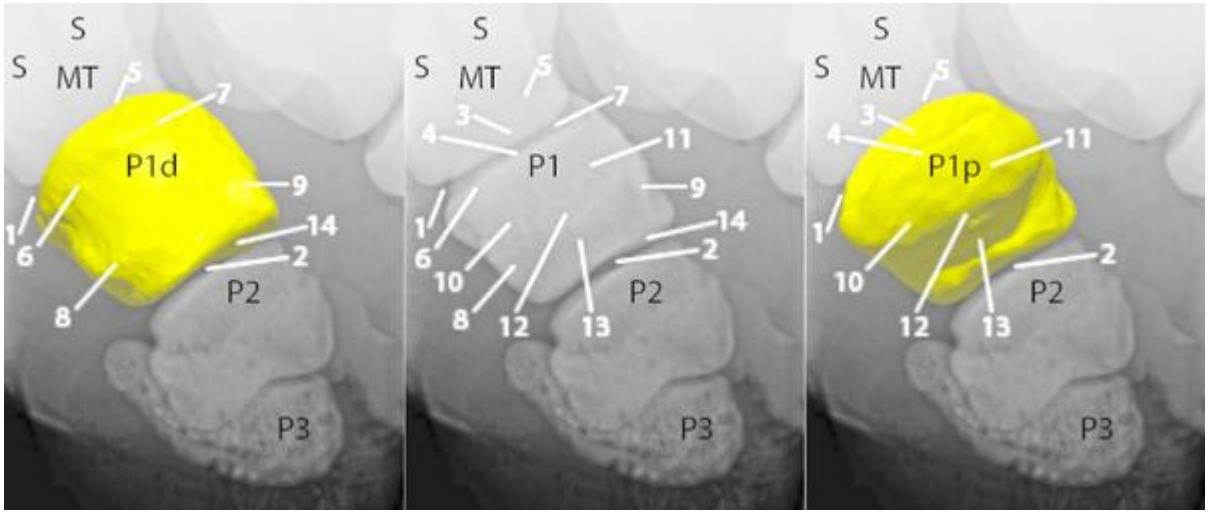

Figure 8: Normal radiographic anatomy of digit II of a white rhinoceros pes, middle phalanx. DIGIT II: MT Metatarsal, P1 Proximal phalanx, P2 Middle phalanx, P2d Middle phalanx dorsomedial aspect, P2p Middle phalanx plantaromedial aspect, P3 Distal phalanx, 1 Proximal interphalangeal joint, 2 Distal interphalangeal joint, 3 Proximal articular surface, 4 Plantaroproximal edge, 5 Dorsoproximal edge, 6 Medial condyle, 7 Lateral condyle, 8 Distal articular surface, 9 Medial oblique ridge, 10 Dorsal transverse recess, 11 Dorsal transverse ridge, 12 Plantar recess 173x111mm (200 x 200 DPI)

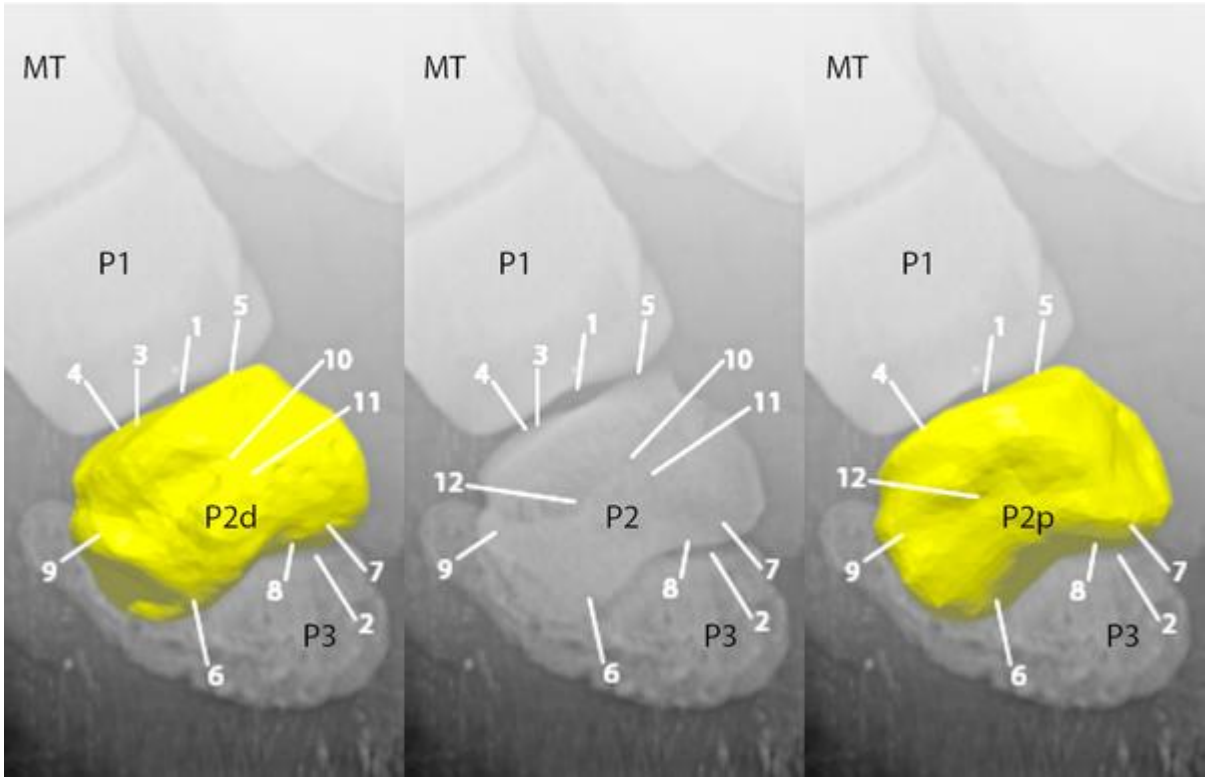

Figure 9: Normal radiographic anatomy of digit II of a white rhinoceros pes, distal phalanx DIGIT II: MT Metatarsal, P1 Proximal phalanx, P2 Middle phalanx, P3 Distal phalanx, P3d Distal phalanx dorsomedial aspect, P3p Distal phalanx plantaromedial aspect, 1 Distal interphalangeal joint, 2 Proximal articular surface, 3 Plantaroproximal edge, 4 Dorsoproximal edge, 5 Planum cuneatum (sole surface), 6 Sole border, 7 Extensor process, 8 Flexor surface, 9 Parietal sulcus, 10 Medial plantar process, 11 Nutrient foramen 173x73mm (200 x 200 DPI)

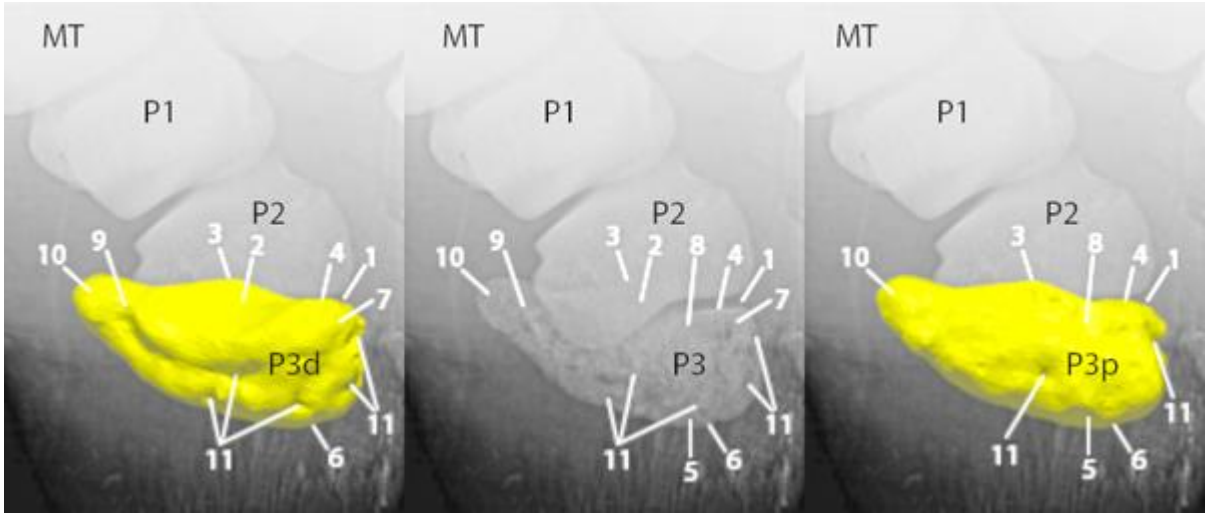

Figure 10: Normal radiographic anatomy of digit IV of a white rhinoceros pes, proximal phalanx. DIGIT IV: MT Metatarsal, P1 Proximal phalanx, P1d Proximal phalanx dorsolateral aspect, P1p Proximal phalanx plantarolateral aspect, P2 Middle phalanx, P3 Distal phalanx, S Proximal sesamoid, 1 Metatarsophalangeal joint, 2 Proximal interphalangeal joint, 3 Proximal articular surface, 4 Plantaroproximal edge, 5 Dorsoproximal edge, 6 Medial dorsoproximal tubercle, 7 Lateral dorsoproximal tubercle, 8 Dorsomedial oblique ridge, 9 Dorsolateral oblique ridge, 10 Medial plantaroproximal tubercle, 11 Lateral plantaroproximal tubercle, 12 Transverse plantar ridge, 13 Transverse plantar groove, 14 Distal articular surface 179x100mm (300 x 300 DPI)

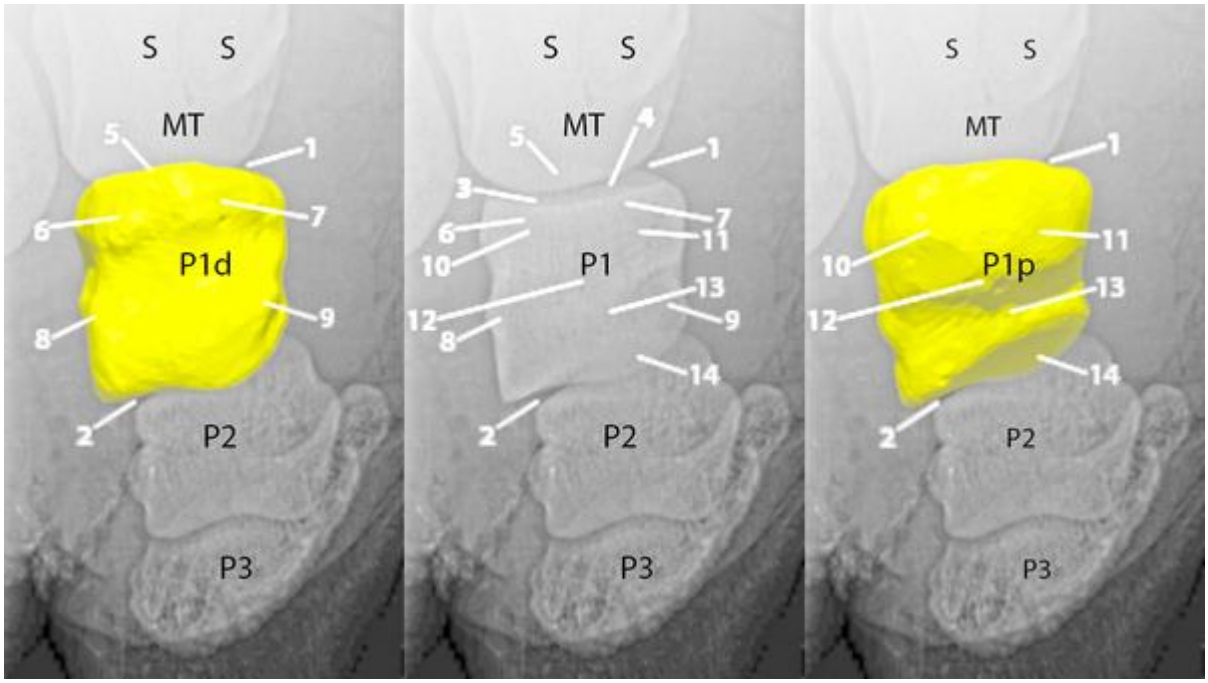

Figure 11: Normal radiographic anatomy of digit IV of a white rhinoceros pes, middle phalanx. DIGIT IV: MT Metatarsal, P1 Proximal phalanx, P2 Middle phalanx, P2d Middle phalanx dorsolateral aspect, P2p Middle phalanx plantarolateral aspect, P3 Distal phalanx, 1 Proximal interphalangeal joint, 2 Distal interphalangeal joint, 3 Proximal articular surface, 4 Plantaroproximal edge, 5 Dorsoproximal edge, 6 Medial condyle, 7 Lateral condyle, 8 Distal articular surface, 9 Medial oblique ridge, 10 Lateral oblique ridge, 11 Dorsal transverse recess, 12 Dorsal transverse ridge, 13 Plantar recess 173x95mm (200 x 200 DPI)

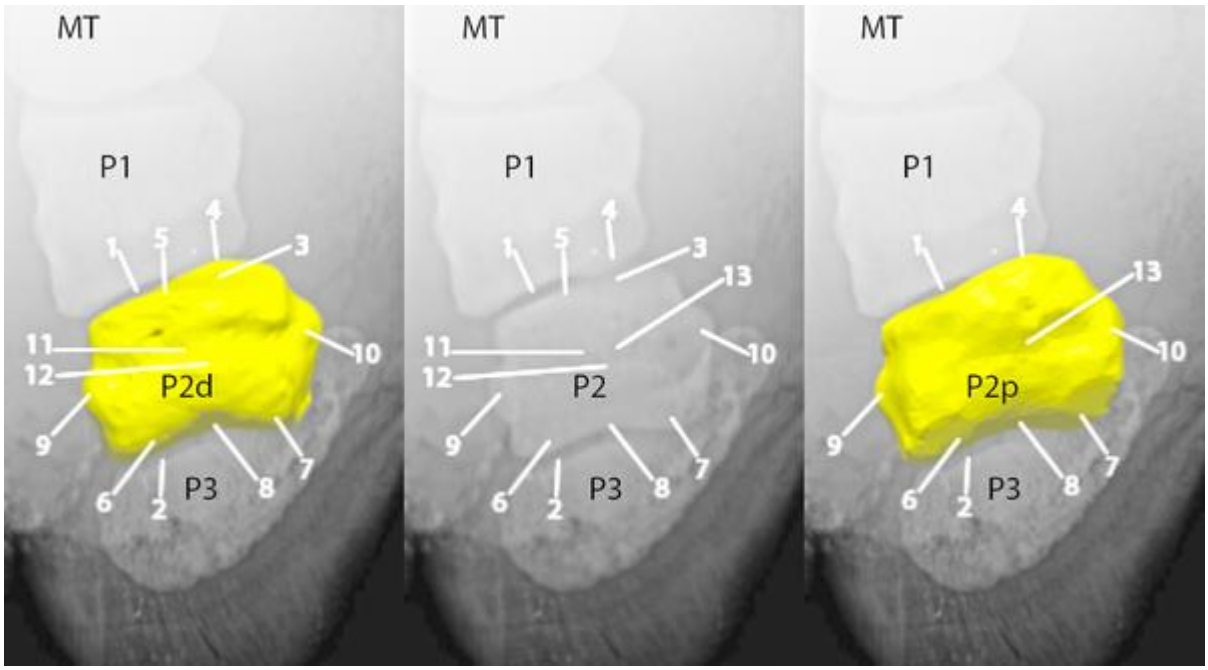

Figure 12: Normal radiographic anatomy of digit IV of a white rhinoceros pes, distal phalanx. DIGIT IV: P1 Proximal phalanx, P2 Middle phalanx, P3 Distal phalanx, P3d Distal phalanx dorsolateral aspect, P3p Distal phalanx plantarolateral aspect, 1 Distal interphalangeal joint, 2 Proximal articular surface, 3 Plantaroproximal edge, 4 Dorsoproximal edge, 5 Planum cuneatum (sole surface), 6 Sole border, 7 Extensor process, 8 Flexor surface, 9 Parietal sulcus, 10 Lateral plantar process, 11 Nutrient foramen 173x74mm (200 x 200 DPI)